Trans Indian Inst Met (2025) 78:36
https://doi.org/10.1007/s12666-024-03529-z

ORIGINAL ARTICLE

Evaluation of Lattice Material Suitability for Additive Manufactured Gears under Compression Loads

Cemal İrfan Çalışkan[1] · Hamaid Mahmood Khan[2] · Gökhan Özer[2] · Mustafa Enes Bulduk[2] · Mert Coşkun[2]

Received: 20 June 2024 / Accepted: 3 September 2024

Abstract Lattice structures have gained increasing prominence in modern applications due to their advantageous traits such as lightweightness, energy absorption capacity without compromising strength. Additive manufacturing processes have further facilitated the integration of lattice structures into components and have opened doors for the development of innovative lattice types. This study focuses on the integration of six distinct lattice forms, comprising both strut-based and TPMS lattice types, into gear blanks. The objective is to evaluate their load-bearing capabilities when the gear teeth are subjected to compression loading. Both numerical simulations and experimental investigations were conducted to analyze the behavior of the tooth-blank system under these conditions. The findings indicate that the incorporation of TPMS structures into the gear blank significantly enhances its resistance to external compression loading compared to the strut-based lattice models. This research highlights the potential of TPMS integration to improve component performance and durability with significant weight reductions in the machinery industry, in various manufacturing sectors, where industrial gears are used. It is thought that high-performance components, which will be produced with AM using less material than traditional production methods, will be used more intensively in future industries.

Keywords Additive manufacturing · Bio-inspired design · Lattice · Laser powder bed fusion (LPBF) · AlSi10Mg

1 Introduction

Compared to industries that often rely on solid metals to achieve strength in large structures, nature also provide solutions that involve cellular forms to optimize functionalities with minimal material consumption [1]. Recognizing these findings has marked a significant advancement in recent times, opening up innovative possibilities across numerous industrial applications and processes. Among these innovations, Additive Manufacturing (AM) technologies have emerged as a transformative field, offering novel perspectives across various industrial domains [15–17].

AM technologies are particularly noteworthy for their ability to produce intricate forms and designs that were previously unattainable through traditional manufacturing methods. These technologies enable the fabrication of internal geometries in complex shapes [13], and their application is expanding across an array of industries [4, 20].

In recent years, a significant amount of literature has been published on AM fabricated lattice materials. For example, [8, 34] researched on several cellular structures, such as auxetic, BCC, and octahedral forms at different angles. TPMS (Triply Periodic Minimal Surface) based lattice materials have also been explored recently in research as well as in several industrial applications [6, 15].

Research on AM prepared Gyroid and Schwartz models have shown positive stress distribution effect in models tested for thermal studies [12]. Moreover, AM prepared lattice materials have also shown remarkable high energy absorption capabilities with reasonable thermo-mechanical properties in many

✉ Cemal İrfan Çalışkan
cemalirfancaliskan@gmail.com

[1] Department of Industrial Design, Istanbul Technical University, Istanbul, Turkey

[2] Aluminum Test, Training, and Research Center, Fatih Sultan Mehmet Vakif University, Halic Campus, 34445 Beyoglu, Istanbul, Turkey

Published online: 11 January 2025

previous works [9, 27, 35]. Research on hybrid lattice materials have also been addressed recently [15]. There are also some bio-inspired lattice studies for various industrial applications, such as innovative bio-inspired fabrics, industrial gear applications, foam applications, and honeycombs [3, 11, 19, 23, 25, 28, and 31].

The integration of AM and lattice materials for industrial gears has allowed the creation of lightweight, strong, and efficient gear components, optimizing material usage, while maintaining mechanical strength [24, 36]. By harnessing the capabilities of AM and lattice structures, industries can enhance gear performance, reduce weight, and contribute to more sustainable and cost-effective manufacturing processes [22, 29]. For example, [22] proposed lightweight metallic AM gears through gear body modifications. Similarly, [21] introduces a lightweight design in tooth, while [2, 14] proposed gears featuring internal cooling channels. Additionally, [26] discusses weight optimization in gears by replacing their full body with a lattice material. Despite extensive research on the static and fatigue properties of AM materials, there is a notable gap in the literature concerning lattice materials integration with the gear system.

Above literature survey has indeed provided strong evidence that lattice structures can significantly influence the performance and durability of industrial gears. Furthermore, it underscores the pivotal role of AM technology in enabling the development of advanced internal lattice forms within gear manufacturing. Building upon these insights, a comprehensive research initiative was developed to explore and quantify the impact of various lattice structures on the mechanical performance of industrial gears.

The present study involved the design of six distinct lattice forms, based on strut-based and TPMS lattice types. The objective was to investigate how these lattice designs would affect the mechanical behavior of gears, specifically focusing on stress transfer from the compressed tooth to the gear blank. A multi-faceted approach encompassing both numerical simulations and experimental investigations was adopted to thoroughly assess the mechanical performance of the gears.

This article, which investigates the usability of different styles of lattice infilled gears in industrial areas, introduces an innovation to the literature within the scope of the comparison of different lattice groups and the manufacturability of industrial gears with AM. The research contains some promising results in comparison of traditional lattice forms and innovative TPMS lattice geometries in industrial gears.

2 Experimental

2.1 Design Process

The Gibson-Ashby mathematical model is instrumental in the design of lattice unit cells for cellular materials [32]. By using the model's equations, designers can tailor the lattice structure's geometry, cell size, and relative density to achieve specific mechanical properties, like stiffness, strength, and weight reduction [5, 18].

The Gibson-Ashby mathematical model fundamentally outlines how the characteristics of a cellular material, such as its density, Young's modulus, and yield strength, are interconnected with its microstructural factors, chiefly the relative density and cell morphology [10].

Mathematically, Gibson-Ashby model can be defined as;

$$\sigma/\sigma_0 = C_1\left(\frac{\rho}{\rho_0}\right)^{n_1} \tag{1}$$

$$E/E_0 = C_1\left(\frac{\rho}{\rho_0}\right)^{n_2} \tag{2}$$

where, E, σ, and ρ are elastic modulus, compressive strength, and density of a solid material. The subscript 'o' signifies the lattice structure in the above equations. Here, $C1$ & $C2$ are constants related to their geometric parameters, $n1$ & $n2$ are exponential factors. The 'C' and 'n' values are typically determined through experimentation and can vary for different materials and manufacturing processes. Once these values are known, the formula can predict the compressive strength of the cellular material based on its relative density [37].

Equations used to create the different TPMS geometries are shared as follows [30]. Here, α is the unit cell size, t is the wall thickness of the gyroid structure [25].

$$\text{Schwarz - P} \quad \cos x + \cos y + \cos z = C \tag{3}$$

$$\text{Schwarz - D} \quad \cos x * \cos y * \cos z - \sin x * \sin y * \sin z = C \tag{4}$$

$$\begin{aligned}\text{Gyroid} \quad & \left(\cos\left(\frac{2\pi}{\alpha}x\right) * \sin\left(\frac{2\pi}{\alpha}y\right)\right. \\ & + \cos\left(\frac{2\pi}{\alpha}y\right) * \sin\left(\frac{2\pi}{\alpha}z\right) \\ & \left. + \cos\left(\frac{2\pi}{\alpha}z\right) * \sin\left(\frac{2\pi}{\alpha}x\right)\right)^2 = t^2\end{aligned} \tag{5}$$

In this ongoing study, we have crafted six unique lattice structures, denoted as BCC (m1), tetrahedral (m2), double pyramid (m3), gyroid (m4), Schwartz d (m5), and Schwarz p (m6). These lattice designs are derived from TPMS forms and have been developed with the specific aim of evaluating how they impact the stability of gear blanks. For a visual representation of these models, please refer to Table 1, which illustrates their schematic representation.

The initial step in the design process was to create models for each of these lattice forms using Catia V5. Subsequently,

these structures were integrated into the gear blank using ANSYS Spaceclaim. It is worth noting that the gear design adheres to the DIN-867 standard, featuring precise dimensions: an outer diameter of 45 mm, an inner diameter of 12 mm, a thickness of 15 mm, and a total of 28 teeth.

The design study involved equalizing the unit volumes of all six models to 3.6 cm^3. It is noteworthy that for all models, both the outer wall thickness and lattice wall thickness were maintained consistently at 0.45 mm. Volume stabilization was achieved by adjusting the intercellular distance. As shown in Table 2, the lattice direction, volume, and thickness values remained consistent across all models, while the cell distance value was varied in each lattice model.

2.2 Static Analysis

The strength analysis of the proposed designs featuring six distinct lattice forms was conducted using ANSYS Discovery Live. This analysis was carried out as a preliminary step before the production of components using the LPBF process. The analysis report was prepared to investigate and understand the impact of compressive strength on gears designed with different TPMS lattice structures. Various stress distribution parameters, including Shear Stress, Principal Stress, and Von-Mises equivalent stress, were evaluated for all the proposed designs.

Notably, in this study, the focus was on analyzing and presenting the Von-Mises stress, as shown in Fig. 1. The Von-Mises stress equation, referred to as Eq. (6) in the study by [33], was employed for this analysis.

$$\sigma = \sqrt{\left[\frac{1}{2}\left((\sigma_{z-}\sigma_r)^2 + (\sigma_{z-}\sigma_\vartheta)^2 + (\sigma_{\vartheta-}\sigma_r)^2\right)\right]} \tag{6}$$

Table 1 Lattice gear designs

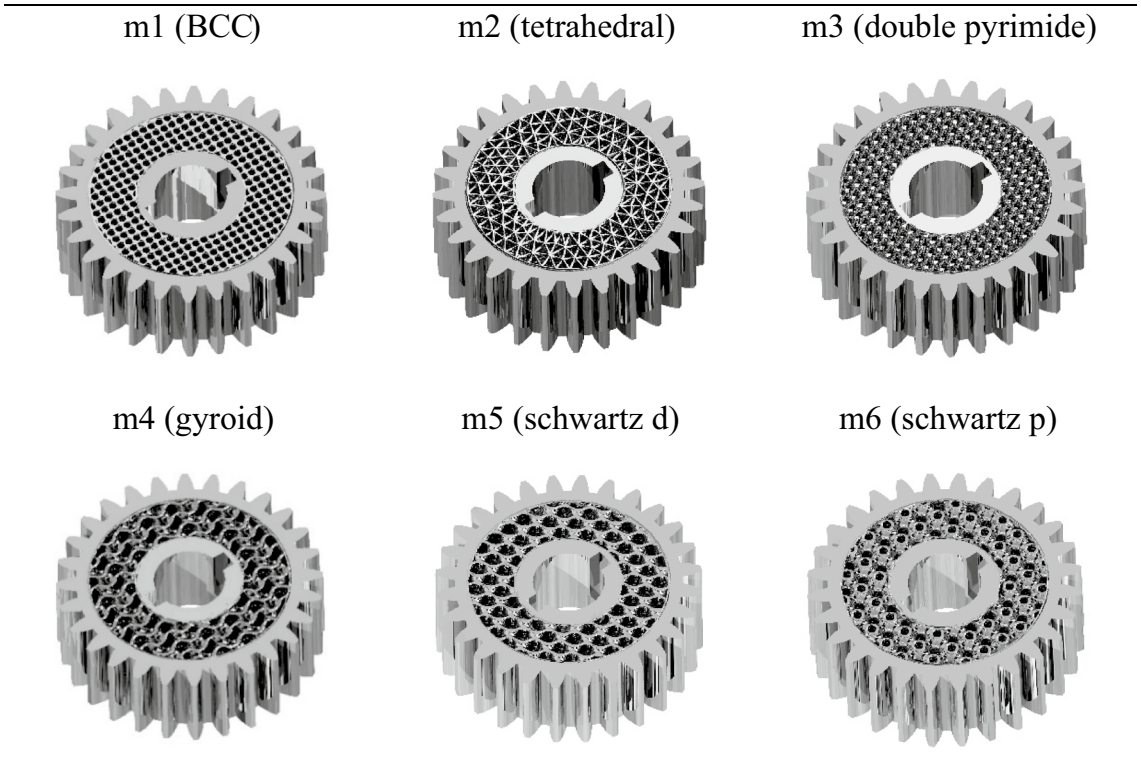

Table 2 Lattice design parameters

Properties	m1	m2	m3	m4	m5	m6
Volume (cm^3)	3.6	3.6	3.6	3.6	3.6	3.6
Outer wall thickness (mm)	0.45	0.45	0.45	0.45	0.45	0.45
Lattice wall thickness (mm)	0.45	0.45	0.45	0.45	0.45	0.45
Lattice cell distance (mm)	1.1	2.4	1.84	1.0	1.24	1.14
Lattice direction	z	z	z	z	z	z

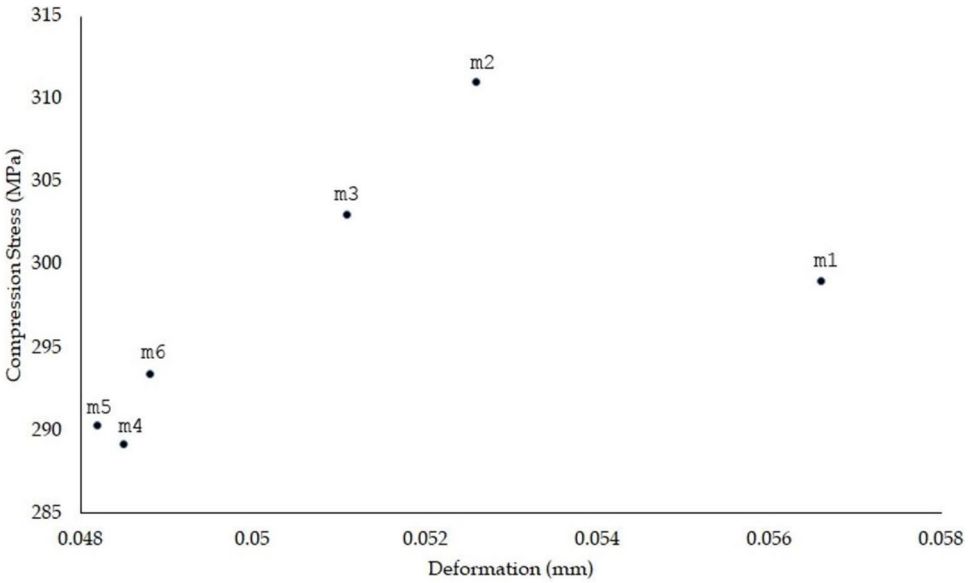

Fig. 1 Results of the analysis study

In this study, the 3D models were saved in the stl file format. When performing FEA, separate mesh structure models were not generated. Instead, the analyses were carried out directly on the existing triangular mesh structures of these models.

Table 3 furnishes details regarding the characteristics of the triangular mesh, including the count of triangles and points utilized in these models.

It is worth noting that the number of meshes varied considerably among the proposed designs, depending on their complexity. Several adjustments and refinements were made to the mesh numbers, and it was observed that these changes did not significantly affect the results.

To expedite the analysis process, the mesh numbers shown in Table 3 were chosen. Regarding boundary conditions, a standard load of 3KN was applied downward onto the tooth surface, as shown in Table 4. To simulate the compression outcomes of the actual apparatus accurately, fixed support conditions were applied to both the gear hub and the bottom teeth.

The graphical representations of the analysis results for all gears are shown in Fig. 1, and a summarized presentation of the results can be shown in Table 4.

Based on the information presented in Fig. 1, it can be observed that when a 3KN load is applied, the maximum stress value falls within a range of approximately 300 ± 10 MPa across various deformation levels for both TPMS and strut-based gear configurations. Upon a closer examination of these two distinct forms, it becomes apparent that TPMS models exhibit a slightly improved stress–strain response, characterized by relatively lesser deformation compared to the strut-based geometries.

As shown in Table 4, it is evident that the stress distributions on both the gear tooth and the gear blank vary among the different models. In this context, the chosen lattice geometries in each model played a pivotal role in determining how stress is distributed across the gear tooth and blank. Notably, models m1–m3 exhibit relatively uniform stress distribution within the blank. In contrast, models m4–m6 display stress reduction patterns closer to the tooth region. This observation suggests that models m4–m6 demonstrated superior stress absorption capabilities compared to models m1–m3.

It is apparent that when moving from the gear tooth to the gear blank, stress levels generally diminish as one approaches the root. The gear blank itself experiences minimal stresses, assuming it is adequately supported and subject to uniform loading. The primary function of the gear blank is to provide support to the gear tooth and transmit the applied loads to the gear shaft. In this particular case, models m4–m6 stand out in their ability to offer substantial support to the gear tooth, resulting in a reduced transfer of stress from the tooth to the blank side. The robust lattice geometry within the gear blank ensures a consistent and stable suppression of stress in models m4–m6.

Table 3 Mesh parameters of the models

	m1	m2	m3	m4	m5	m6
Triangles mesh number	1,100,268	354,976	972,018	2,344,998	1,389,054	1,826,454
Point number	539,934	162,914	459,294	1,171,351	693,269	911,875

Table 4 Analysis result images of six models, stress distributions

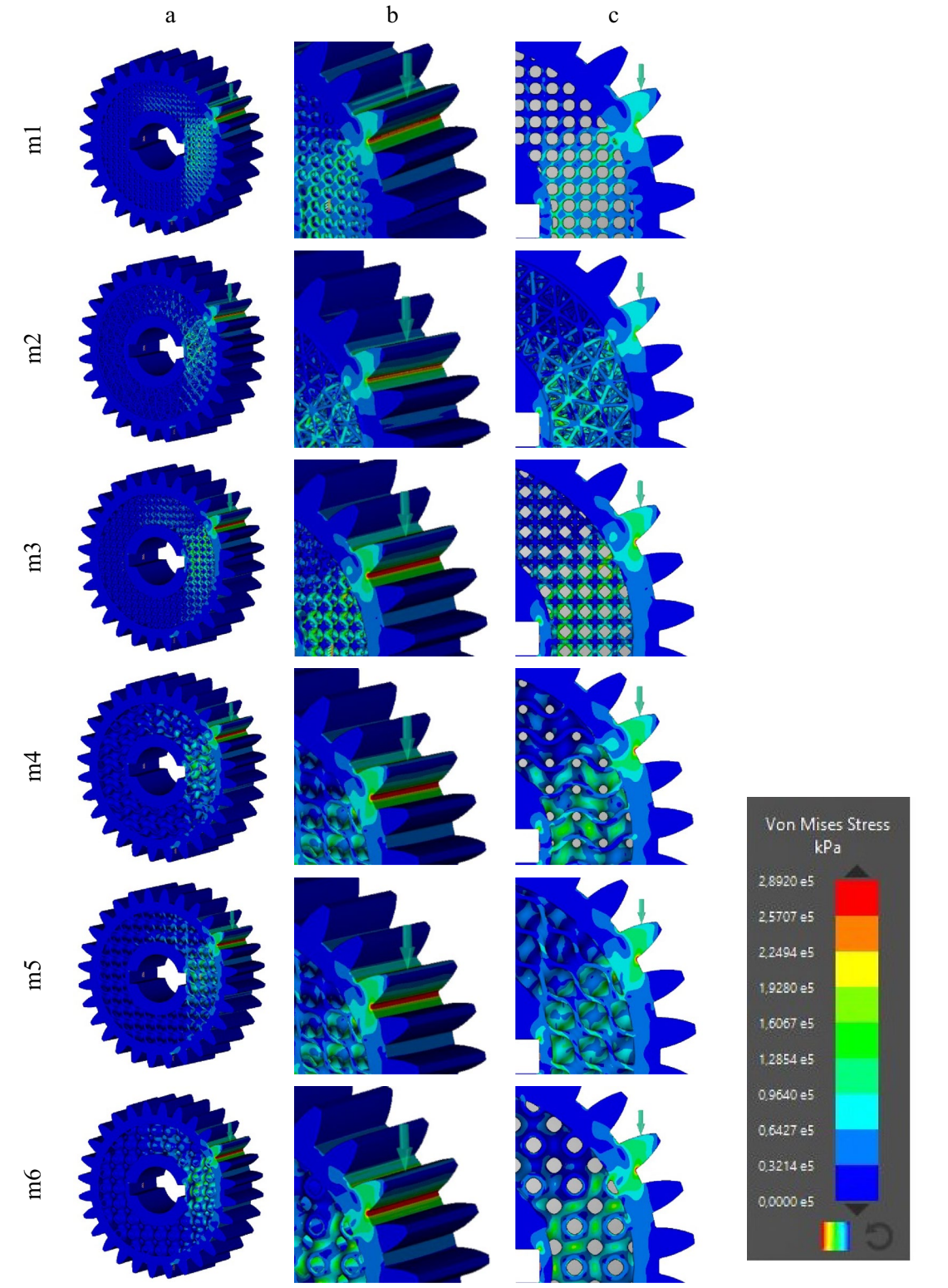

Fig. 2 Bio-inspired lattice gears as prepared on the EOS M290 LPBF machine

Table 5 LPBF production parameters for AlSi10Mg [7]

Laser power	Scan speed	Hatch distance	Layer thickness
370W	1300 mm/s	0.19 mm	30 µm
Preheat temperature	Laser intensity	Scanning strategy	
35 °C	49,93 J/mm^3	x-rotation	
Laser type	Atmosphere	Global beam offset	Part beam offset
Ytterbium Fibre	Argon	0.1 mm	0.02 mm

2.3 LPBF Production and Compression Test

Following the preliminary model design and the numerical analysis stage, the six gear models were fabricated using AlSi10Mg material on a metal 3D printer (EOS M290), as shown in Fig. 2. These gear models were strategically arranged in a horizontal orientation on the production platform and were manufactured efficiently in a single production run. Subsequently, they were subjected to standard compression testing to assess their mechanical properties and performance under load.

The manufacturing of gear models using AlSi10Mg material followed the recommended standard laser processing parameters as specified by EOS, which are comprehensively shown in Table 5. In addition, Table 6 presents the material properties of AlSi10Mg.

The fabricated gears underwent compression testing on ALSA 100 KN, Turkey within the designated test setup (Fig. 3a). Subsequently, deformation and fracture analysis were conducted using a Scanning Electron Microscope (SEM) setup, as shown in Fig. 3b. Notably, no postprocessing was applied following the removal of supports.

In the SEM study, fracture analysis was conducted on all gear models, utilizing magnifications of 35, 100, and 500 times, employing a Hitachi SU 3500 microscope. This analysis aimed to elucidate the differences in deformation characteristics among industrial gears with distinct lattice types.

3 Results

All of the gear models underwent compression testing, and their behavior during deformation at 2 and 4 mm was meticulously recorded through video documentation. Table 7 provides a visual representation of the position of each compressed gear at 2 and 4 mm of compression for all the models. It is noteworthy that nearly all gear models exhibited signs of deformation at the 2 mm compression stage, indicating an early onset of compression.

However, the deformation characteristics of each model, particularly between models m1–m3 and m4–m6, displayed notable differences in each case. While all proposed gear models demonstrated a ductile mode of failure, the stress distribution during the progression of the compression test significantly varied between the two sets of gear models.

As emphasized earlier, models m4–m6 exhibited a remarkable ability to withstand the compression load,

Table 6 Material properties of AlSi10Mg [15]

Density (ISO3369)	Yield strength (vert.) ISO 6892-1	Yield strength (hor.) ISO 6892-1
≥ 2.67 g/cm3	230 MPa	270 MPa
Tensile strength (vert.) ISO 6892–1	Tensile strength (hor.) ISO 6892-1	Particle size distribution
460 MPa	450 MPa	25–70 µm
Average defect percentage as manufactured	Elongation at break (vert.) ISO 6892-1	Elongation at break (hor.) ISO 6892-1
%0.04	%6.3	%10.2

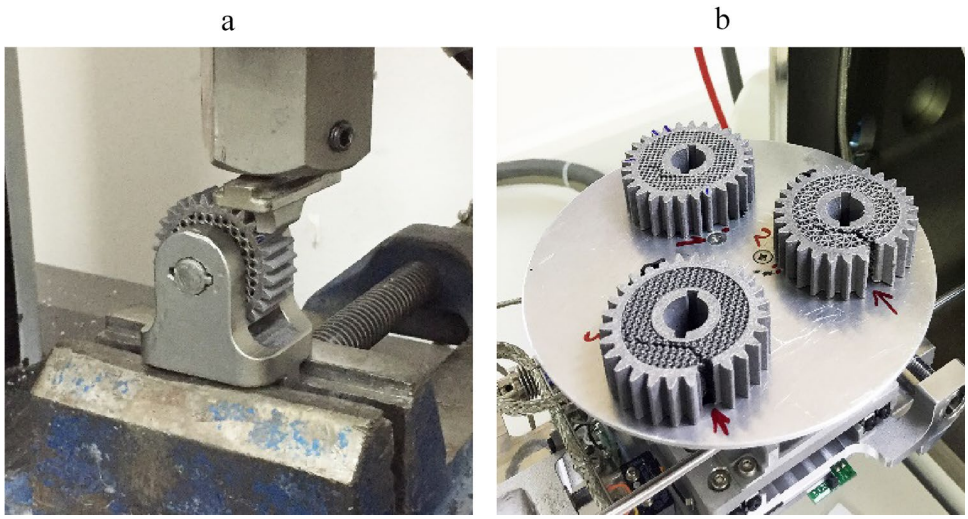

Fig. 3 **a** Compression test setup, **b** SEM study

Table 7 Deformation images of six lattice gear models at 2 and 4 mm

	m1	m2	m3
Deformation of the gear at **2 mm** compression	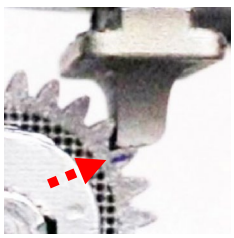	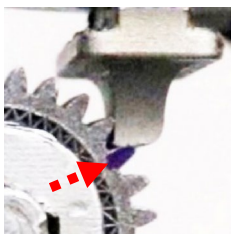	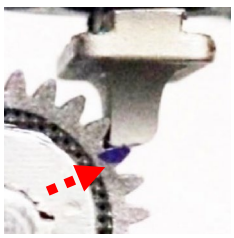
At **4 mm** compression	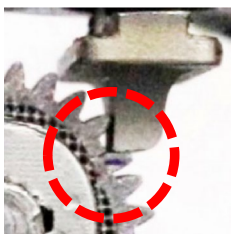		
	m4	**m5**	**m6**
At **2 mm** compression	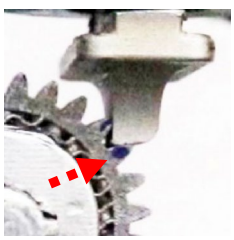	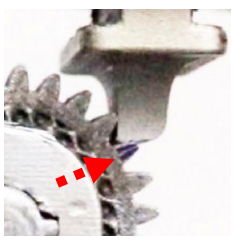	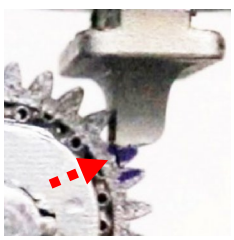
At **4 mm** compression	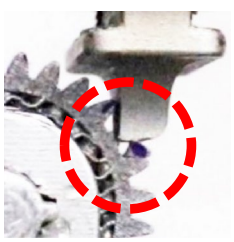	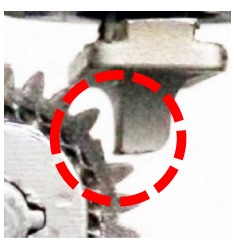	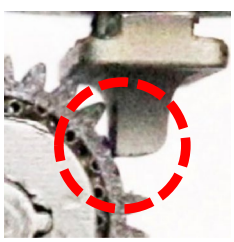

resulting in the gear blank remaining intact, while the gear itself experienced failure. In contrast, gear models within the m1–m3 set were unable to resist the compression load, leading to the fracture of the gear blank. This situation is unfavorable as it can potentially lead to catastrophic machine component failure, resulting in significant property damage and even potential safety risks.

The video recording examination is insufficient to determine the fracture types of proposed gear models. Consequently, it become evident that a more detailed analysis is necessary, prompting the need for SEM assessment at various magnification levels for all gear models.

Figure 4 illustrates the relationship between applied stress and deformation for all gear types, revealing distinct behaviors between the two gear sets. Models m1–m3 exhibited a significant onset of permanent deformation at approximately 1.25 mm compression and around 6500–8000N of applied compression load. Notably, models m1 and m3 continued to undergo expansion of more than 1.5 mm even with a constant load, which can be attributed to the load being transferred from the gear tooth to the gear blank, resulting in rapid rupture. The gear blank in these models failed to provide the necessary support to the tooth under compression, leading to the gear's fracture.

In contrast, models m4–m6 displayed a higher stress-bearing capacity of about 9000–10000N before reaching the onset of permanent deformation. As indicated in Fig. 4, the deformation mode in these models was sudden, unlike the gradual expansion observed in models m1 and m3. This difference in deformation behavior can be attributed to the robust nature of the gear blank in models m4–m6. The stress generated at the gear tooth during the compression test was predominantly contained within the tooth region and distributed only minimally to the gear blank. Consequently, the gear tooth broke, while the blank remained stable.

The deformation mode displayed by models m4–m6 is preferable in a gear assembly as it can prevent abrupt machine part failure, thus safeguarding the entire machinery. In contrast, when cracks propagate into the gear blank from the tooth, as observed in models m1 and m3, this type of deformation can be catastrophic for the machine component.

Aluminum, as is known, is a material that exhibits elastic–plastic deformation. This type of deformation is expressed by Hooke's law (7).

$$\sigma = E\varepsilon \tag{7}$$

In this study, it is seen that the material exhibits plastic behavior since it is determined that it gets fractured. Therefore, the stress and strain diagram is given according to Hooke's law (Fig. 4). In addition, the maximum stress values of the six gear model were shared as Table 8.

Table 9 offers SEM images that provide insights into the failure modes and behaviors of the gear models. As mentioned earlier, it is clear that the deformation mode of each gear model

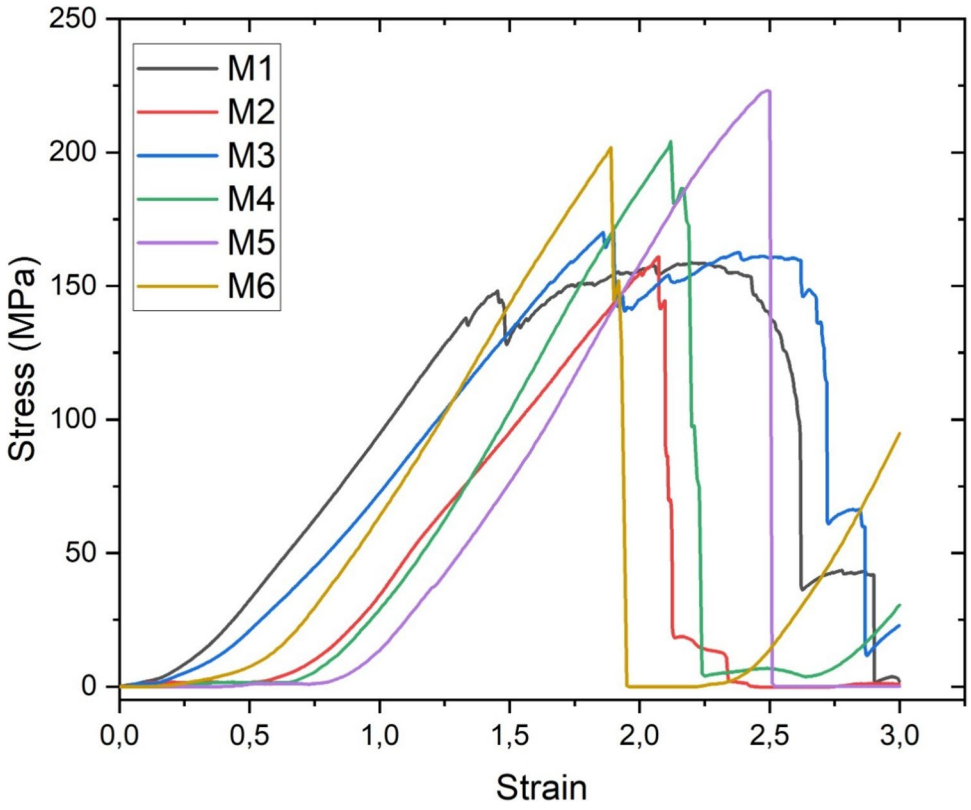

Fig. 4 Compression test result graph for six lattice models

Table 8 Maximum stress values of the models

	m1	m2	m3	m4	m5	m6
Maximum Stress(MPa)	158.667	160.956	162.578	204.15	223.156	201.782

Table 9 SEM surface examination of six lattice gear models and fracture analysis

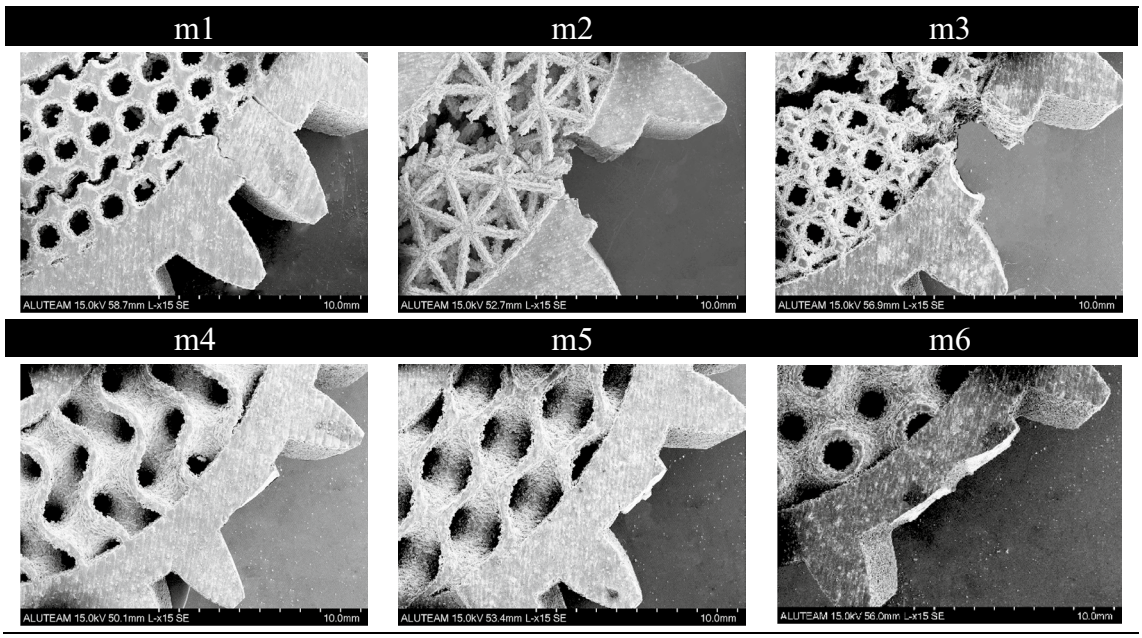

is fundamentally ductile in nature, although the extent of ductility varies among the different cases.

The examination of gear blanks in Table 9 clearly reveals distinct behaviors between models m1–m3 and models m4–m6. In the case of models m1–m3, the gear blanks can be observed tearing apart under the applied compression loading, indicating their relatively weaker strength to withstand external stresses in dynamic operational conditions.

Conversely, the gear blanks of models m4–m6 remained stable and uncracked during the tests, with only the gear tooth bearing the maximum stress from the compression load. This observation underscores the robustness of the gear blanks in models m4–m6, as they effectively prevent the propagation of cracks from the tooth to the blank region. It is known that a stronger gear blank provides greater support to the gear tooth, making it more resistant to deformation. This can result in reduced tooth deflection or bending when subjected to load. Consequently, it can be expected that stress distribution in models m4–m6 is more uniform and less localized compared to models m1–m3, which experienced gear rupture due to localized stress concentrations.

4 Discussion

Additive manufacturing processes, especially those involving LPBF techniques, are continuously evolving within the industrial sector. This is largely attributed to their advantages in material handling and parts fabrication. However, it is important to acknowledge that conventional manufacturing methods have a rich history, with products having undergone extensive testing and modification to meet the demands of various applications.

While AM products represent a relatively novel approach, there is still a need for thorough investigation to ensure their suitability for current industrial requirements. In this particular study, we focus on the incorporation of lattice materials produced through the LPBF process into gear geometry. Notably, modifications have been implemented on the blank side of the gear to assess their impact on the tooth geometry.

It is well understood that the gear blank primarily serves as a foundation for the gear tooth, facilitating the transmission of applied loads to the gear shaft. Additionally, the gear blank plays a crucial role in evenly distributing these

transmitted loads and stresses across the entire structure of the gear. Proper design and material selection for the gear blank are essential in achieving even load distribution and minimizing localized stress concentrations.

It is crucial to emphasize that the material used for the gear blank must possess the necessary mechanical properties, including hardness, toughness, and wear resistance, to endure the loads and stresses encountered during operation. The quality and properties of the gear blank material directly impact the strength of the gear tooth.

Previous review studies have extensively explored the strength of gyroid TPMS, especially when compared to other strut-based lattice models. This comparison could also explain their superior resistance to external compressive loading in TPMS models m4–m6 when contrasted with strut-based models (m1–m3). This insight underscores the importance of selecting the appropriate lattice structure for optimizing the performance of AM-manufactured components in various industrial applications.

5 Conclusions

Based on the comprehensive analysis and compression tests conducted on industrial gears incorporating six distinct lattice forms, several significant findings emerge:

- The integration of strut-based lattice structures (m1–m3) within gear blanks exhibited failure under compression loading conditions. In contrast, TPMS models (m4–m6) demonstrated remarkable resistance to compression stress, leading to tooth fracture, while maintaining the stability of the gear blank itself.
- TPMS lattice materials consistently demonstrated superior stress-bearing capabilities during compression testing. These lattice structures effectively delayed the onset of permanent deformation compared to the strut-based lattice models. This enhanced resilience is crucial for industrial gears exposed to heavy loads.
- TPMS lattice forms have proven to be better suited for industrial gear applications, particularly in terms of mechanical strength and deformation behavior. They allow gears to continue functioning with minimal damage to the gear assembly, which is essential in industrial systems, where operational uptime is critical.
- The ability of TPMS lattice models to limit damage to the gear assembly contributes to cost-effective and efficient gear systems. By preserving the integrity of other components within the system, they ensure extended operational periods and reduce maintenance costs.

The selection of the lattice type in industrial gear design has a profound impact on performance, durability, and the potential for damage to other system components. This research underscores the significance of choosing appropriate lattice forms and emphasizes the advantages of innovative lattice structures, such as TPMS, in optimizing industrial gear applications. Such advancements not only enhance mechanical strength but also ensure reliable, long-lasting gear systems in various industrial settings.

Authors Contributions Cemal İrfan Çalışkan was involed in introduction, design process, experimental, discussion result section authorship, CAD modeling, and table studies; Hamaid Mahmood Khan was involed in analysis and numerical methodology, result and discussion and conclusion authorship; Gökhan Özer: SEM was involed in lab. works and translation, introduction authorship contribution; Mustafa Enes Bulduk was involed in lab. studies, Mert Coşkun was involed in LPBF productions, static analysis and section authorship contribution.

Funding The additive manufacturing productions of this study were supported within the scope of the "Aluteam: Joint Research Center Project for the Digital Transformation of the Aluminum Industry", which is a European Union Project (IPA) supported by the Ministry of Industry and Technology, Directorate General for EU Affairs and the European Union Financial Programs Department of Foreign Affairs. In addition, the design studies of the research were carried out within the scope of ITU Scientific Research Project ID: 45766.

Data Availability The authors confirm that the data and material supporting the findings of this work are available within the article.

Declarations

Conflict of interest We declare that we have no financial and personal relationships with other people or organizations that can inappropriately influence our work, this is no professional or other personal interest of any nature of kind in any product, service and/or company that could be constructed as influencing the position presented in, or other review of, the manuscript entitled.

Ethical Approval The article follows the guidelines of the Committee on Publication Ethics (COPE) and involves no studies on human or animal subjects.

Consent to Participate Not applicable. The article involves no studies on humans.

Consent to Publish Not applicable. The article involves no studies on humans.

References

[1] Ashby M F, and Medalist R F M, *Metall Trans A* **14** (1983) 1755.
[2] Bräunig J, Töppel T, Müller B, Burkhardt M, Hipke T, and Drossel W-G, *Adv Mech Eng* **6** (2014) 741083.
[3] Bulduk M E, Çalışkan C İ, Coşkun M, Özer G, and Koç E, *Int J Adv Manuf Technol* **119** (2022) 6707. https://doi.org/10.1007/s00170-021-08405-4
[4] Çalışkan C İ, and Arpacıoğlu Ü, *Rapid Prototyp J* **28** (2022) 1808.

[5] Chua C, Sing S L, and Chua C K, *Virtual Phys Prototyp* **18** (1), (2023) e2138463.
[6] Ejeh C J, Barsoum I, and Al-Rub R K A, *Int J Mech Sci* **223** (2022) 107293.
[7] EOS, *EOS Aluminium AlSi10Mg Material Data Sheet*, (2022)
[8] Erturk A T, Bulduk M, Tarakçi G, Özer G, and Yarar E, *Metals Mater Int* **28** (1), (2022) 155.
[9] Gawronska E, and Dyja R, *Materials* **14** (2021) 427.
[10] Gibson L J, Ashby M F, *Cellular solids: Structure and properties*. Cambridge University Press (2014). https://doi.org/10.1017/CBO9781139878326
[11] Herman M J, Peterson D, Henderson K, Cardenas T, Hamilton C E, Oertel J, and Patterson B M, *Fus Sci Technol* **73** (2018) 166.
[12] Hussein A, Hao L, Yan C, Everson R, and Young P, *J Mater Process Technol* **213** (2013) 1019. https://doi.org/10.1016/j.jmatprotec.2013.01.020
[13] Kamps T, Gralow M, Schlick G, and Reinhart G, *Procedia Cirp* **65** (2017) 259.
[14] Kamps T, Reinhart G, *Increasing transmission efficiency by implementation of a conformal cooling system using additive manufacturing*, (2014)
[15] Khan H M, Çalışkan C İ, and Bulduk M E, *3D Print Addit Manuf.* **10** (2023) 1371. https://doi.org/10.1089/3dp.2022.0224
[16] Khan H M, Karabulut Y, Kitay O, Kaynak Y, and Jawahir I S, *Mach Sci Technol* **25** (2021) 118. https://doi.org/10.1080/10910344.2020.1855649
[17] Khan H M, Özer G, Yilmaz M S, and Koc E, *Arab J Sci Eng* **47** (2022) 5465. https://doi.org/10.1007/s13369-021-06481-y
[18] Kornievsky A, and Nasedkin A, *Materialia* **26** (2022) 101563.
[19] Li S, Bai H, Shepherd R F, and Zhao H, *Angew Chem Int Ed* **58** (2019) 11182.
[20] Majeed M, Khan H M, Wheatley G, and Situ R, *J Braz Soc Mech Sci Eng* **44** (2022) 389. https://doi.org/10.1007/s40430-022-03703-8
[21] Muminovic AJ, Colic M, Mesic E, Saric I, *Bull Polish Acad Sci Tech Sci*, (2020)
[22] Mura A, Curà F, and Pasculli L, *Proc Inst Mech Eng Part C J Mech Eng Sci* **232** (2018) 3512. https://doi.org/10.1177/0954406217737107
[23] Nagel J K S, Schmidt L, and Born W, *Designs* **2** (2018) 47.
[24] Nguyen L H, and Nguyen K T, *J Mach Eng* **22** (2022) 21.
[25] Pan C, Han Y, and Lu J, *Appl Sci* **10** (2020) 6374.
[26] Ramadani R, Belsak A, Kegl M, Predan J, and Pehan S, *Int J Simul Model* **17** (2018) 92.
[27] San Ha N, and Lu G, *Compos Part B Eng* **181** (2020) 107496.
[28] Schneider J, Schiffer A, Hafeez F, and Kumar S, *Int J Mech Sci* **219** (2022) 107126.
[29] Shweiki S, Palermo A, and Mundo D, *Shock Vib* **1** (2017) 7982170.
[30] Simsek U, Gayir C, Kavas B, in *Sim-AM 2019: II International Conference on Simulation for Additive Manuf*, CIMNE (2019), p 369
[31] Singh A V, Rahman A, Kumar N S, Aditi A S, Galluzzi M, Bovio S, Barozzi S, Montani E, and Parazzoli D, *Mater Des* **1980–2015** (2012) 829.
[32] Uhlířová T, and Pabst W, *Scr Mater* **159** (2019) 1.
[33] Wang Y-Z, Li G-Q, Wang Y-B, and Lyu Y-F, *J Constr Steel Res* **181** (2021) 106624.
[34] Wu Y, and Yang L, *Int J Mech Sci* **197** (2021) 106325.
[35] Xiao L, Xu X, Feng G, Li S, Song W, and Jiang Z, *Int J Mech Sci* **219** (2022) 107093. https://doi.org/10.1016/j.ijmecsci.2022.107093
[36] Xu G, and Dai N, *Math Biosci Eng* **18** (2021) 1653.
[37] Xu Y, Zhang D, Hu S, Chen R, Gu Y, Kong X, Tao J, and Jiang Y, *J Mech Behav Biomed Mater* **99** (2019) 225.